ACS APPLIED MATERIALS & INTERFACES

Research Article

www.acsami.org

Facile Fabrication of N-Doped Graphene as Efficient Electrocatalyst for Oxygen Reduction Reaction

Yongliang Liao,[†,⊥] Yuan Gao,[‡,§,⊥] Shenmin Zhu,[*,†] Junsheng Zheng,[‡,§] Zhixin Chen,[∥] Chao Yin,[†] Xianghong Lou,[†] and Di Zhang[†]

[†]State Key Laboratory of Metal Matrix Composites, Shanghai Jiao Tong University, 800 Dongchuan Road, Shanghai 200240, People's Republic of China

[‡]Clean Energy Automotive Engineering Center and [§]School of Automotive Studies, Tongji University (Jiading Campus), 4800 Caoan Road, Shanghai 201804, People's Republic of China

[∥]The Faculty of Engineering and Information Sciences, University of Wollongong, Wollongong, New South Wales 2522, Australia

Supporting Information

ABSTRACT: A facile bottom-up method is reported here for the fabrication of N-doped graphene for oxygen reduction. It consists of a two-step calcination strategy and uses α-hydroxy acids (AHAs) as carbon source and melamine as nitrogen source. Three different AHAs, malic acid, tartaric acid, and citric acid, were chosen as the carbon sources. The prepared N-doped graphenes have a typical thin layered structure with a large specific surface area. It was found that the N content in the obtained N-doped graphenes varies from 4.12 to 8.11 at. % depending on the AHAs used. All of the samples showed high performance in oxygen reduction reaction (ORR). The N-doped graphene prepared from citric acid demonstrated the highest electrocatalytic activity, which is comparable to the commercial Pt/C and exhibited good durability, attributing to the high pyridinic N content in the composite.

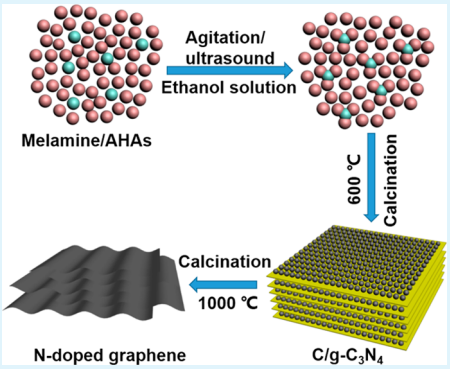

KEYWORDS: *N-doped graphene, ORR, fuel cells, α-hydroxy acids, bottom-up method*

INTRODUCTION

Fuel cells have drawn worldwide attention because of their high efficiency of energy conversion, quick start-up, and low emission of toxic gases. The electrochemical performance of a fuel cell depends largely on the oxygen reduction reaction (ORR), which is substantially determined by the catalytic activities of the cathode catalysts because of the sluggish reaction kinetics of ORR.[1] Platinum (Pt) and Pt-based materials have been commonly used as cathode catalysts for ORR,[2−7] owing to their low overpotential and high catalytic activity. Unfortunately, their applications are limited by high cost, time-dependent drift, and poor durability.[8,9] Therefore, developing a low cost and efficient catalyst to substitute a Pt-based electrode turns out to be an important task.

As a two-dimensional (2D) monolayer carbon material consisting of sp^2 carbon atoms, graphene is of great interest for its potential applications in nanoelectronics,[10] in energy storage,[11] as supercapacitors,[12,13] as sensors,[14] and so on. However, perfect graphene does not show any performance in ORR because it does not have a band gap. Doping with heteroatoms turns out to be an effective approach to gain some performance in ORR, which has been proved by both theoretical calculations and detailed experiments.[15] For instance, N doping in graphene can create positive charge sites to attract oxygen, thus modulating the electronic structure of graphene and then giving the ORR performance. As a result, the N-doped graphene or other carbon materials have shown high ORR performance in both alkaline media and acidic media[16] and long durability[17] as well as good methanol tolerance.[18] Various approaches have been developed for the synthesis of N-doped graphene to replace the expensive Pt-based catalysts.[19] These include chemical vapor deposition (CVD),[20,21] thermal annealing graphene oxide (GO) method with NH_3 or nitrogen-containing organics as the nitrogen source.[22,23] In CVD, metal catalysts are used to transfer organic molecules to graphene but metal contamination can negatively influence the performance of ORR. Moreover, NH_3 and pyridine used in the CVD process are toxic and dangerous. In terms of thermal annealing method, strong acid and oxidant should be used to chemically exfoliate graphite to GO. Recently, a bottom-up approach synthesis from small precursor molecules opens a new way to prepare graphene or N-doped graphene.[24,25] In this process, glucose is generally used as the carbon source. As a carbon source, organic acids are more attractive as compared with glucose, owing to the existence of acid groups. The acid groups can react with amino groups of melamine or dicyandiamide to reinforce the connection between carbon source and nitrogen source to form N-doped

Received: April 17, 2015
Accepted: August 20, 2015
Published: August 20, 2015

DOI: 10.1021/acsami.5b05649
ACS Appl. Mater. Interfaces 2015, 7, 19619−19625

Scheme 1. Proposed Synthetic Protocol for N-Doped Graphene

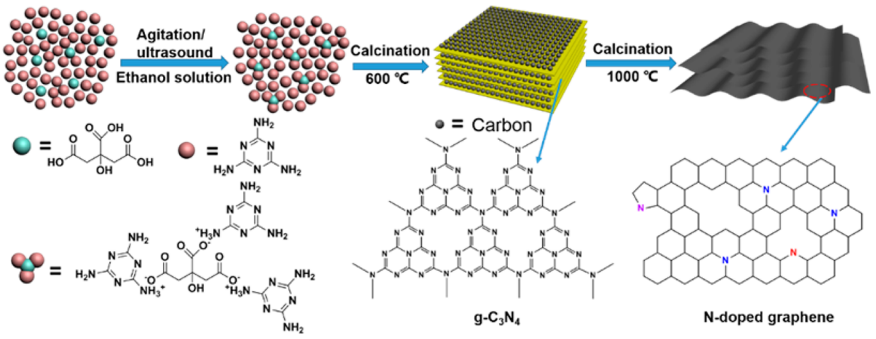

graphene. Among various organic acids, α-hydroxy acids (AHAs) are abundant in fruits and harmless. A hypothesis made herein is that AHAs can be chosen as carbon sources to prepare N-doped graphene with high quality.

Here we report a facile bottom-up approach to prepare N-doped graphene using AHAs as carbon sources and melamine as nitrogen source. In this research, malic acid, tartaric acid, and citric acid are chosen as typical AHAs used as carbon sources, because they widely exist in common fruits such as apples, grapes, and lemons, etc. During the processes, they can react with melamine to form organic salts to enhance the connection between the carbon source and the nitrogen source, which makes them ideal carbon sources. The as-prepared N-doped graphenes would have high specific surface areas, high nitrogen contents, and mesoporous architectures, which would result in exhibiting much enhanced ORR catalytic activity and high durability.

EXPERIMENTAL SECTION

Materials and Synthesis. Analytic grade reagents including melamine, L-malic acid, L(+)-tartaric acid, citric acid, and alcohol were purchased from Sinopharm Chemical Reagent Co., Ltd. The typical N-doped graphenes were prepared by calcining the precursors made from melamine and various AHAs. In specific, 1 g of AHAs (L-citric acid, L(+)-tartaric acid, or malic acid) and 35 g of melamine were added into 150 mL of ethanol and stirred at ambient temperature for 20 min, followed by sonication (20 kHz, 600 W) in an ice-water bath using a probe type ultrasonic processor for 15 min. Then the suspension was stirred in a water bath at 60 °C until no obvious liquid could be found. White aggregates were obtained after drying the powders at 60 °C for 24 h. Then the white aggregates were transferred into a ship crucible (100 cm × 50 cm × 50 cm) with a cover and calcined at 600 °C for 2 h at a heating rate of 2.3 °C/min. The intermediate products were then heated to 1000 °C at a heating rate of 3.3 °C/min and kept at this temperature for another 1 h. All the procedures were operated in N_2 atmosphere. After cooling to room temperature, the N-doped graphene samples were thus obtained. The N-doped graphenes prepared from the three different AHAs—malic acid, tartaric acid, and citric acid (their molecular formulas are shown in Scheme S1)—are denoted as NG-M, NG-T, and NG-C, respectively.

Characterization. Field-emission scanning electron microscopy (FESEM) was performed on a JEOL JSM-6360LV field-emission microscope at an accelerating voltage of 15 kV. Transmission electron microscopy (TEM) and high-resolution TEM (HRTEM) were operated on a JEOL 2011F microscope at 200 kV. Atomic force microscopy (AFM) measurements were performed on a Nanonavi E-Sweep N environment control scanning probe microscope. X-ray diffraction (XRD) was conducted on a RigakuD/max2550VL/PC system at 40 kV and 40 mA with Cu Kα radiation (λ = 1.5406 Å), at a scan rate of 5° min^{-1} and a step size of 0.050° in 2θ. Raman spectroscopy was conducted on a Senterra R200-L dispersive Raman microscope with 532 nm laser excitation. Nitrogen adsorption measurements at 77 K were accomplished using an ASAP2020 volumetric adsorption analyzer, after the samples had been outgassed for 8 h in the degas port of the adsorption apparatus. The specific surface area was calculated by applying the Brunauer–Emmett–Teller (BET) model to the isotherm data points of the adsorption branch. X-ray photoelectron spectroscopy (XPS) was carried out on a ThermoFisher K-Alpha X-ray photoelectron spectrometer with a lateral resolution of 400 μm.

Electrochemical Measurement. The ORR activities were measured on a CHI 750C (CH Instrument Inc., Austin, TX, USA) which is equipped with a three-electrode system in O_2-saturated 0.1 M KOH solution. Glassy carbon (GC, 5.61 mm in diameter) electrode coated with the as-prepared catalysts' ink was used as the working electrode. An Ag/AgCl electrode was used as the reference electrode, and a platinum plate was used as the counter electrode. The working electrode was produced as follows: 2 mg of the as-prepared catalyst was added into a 1 mL mixture of Nafion solution (5 wt %, DuPont) and methanol. The solution was ultrasonicated for 2 h to obtain a homogeneous suspension ink. Then 10 μL of the catalyst ink was pipetted twice onto the surface of the GC electrode to form a thin catalyst film on the GC electrode. After drying in ambient air, the working electrode was placed on the rotating pole for experiments. The cyclic voltammetry (CV) and linear sweep voltammetry (LSV) were carried out to obtain the potential–current curves with which the catalyst electrochemical performance and the catalyst durability were evaluated.

RESULTS AND DISCUSSION

Properties of N-Doped Graphene. The preparation procedure for N-doped graphene is depicted in Scheme 1. First, AHA (taking citric acid for example) was mixed with an excessive amount of melamine under ultrasonication, during which organic salt formed and dispersed in melamine suspension. After the calcination at 600 °C, layered graphitic carbon nitride (g-C_3N_4) was obtained from the pyrolysis of the melamine,[26] which bonded with the as-formed aromatic carbon intermediates from the decomposition of the organic salt (the XRD pattern and SEM image of the g-C_3N_4 are shown in SI Figures S1 and S2). In the calcination at 1000 °C, the obtained g-C_3N_4 gradually decomposed while the carbon retained the layered structure and crumpled to form graphene with N atoms doped into the carbon frameworks. The resultant materials obtained from the malic acid, tartaric acid, and citric acid are corresponding to NG-M, NG-T, and NG-C, respectively.

As shown in Figure 1a, the obtained N-doped graphenes from the citric acid (NG-C) presents a typical thin layered and wrinkled structure. The thin nanosheets are further confirmed by TEM images (Figure 1b). A higher magnification image in Figure 1c demonstrates a flake-like and crumpled structure, which agrees well with the SEM results. A selected area electron

DOI: 10.1021/acsami.5b05649
ACS Appl. Mater. Interfaces 2015, 7, 19619–19625

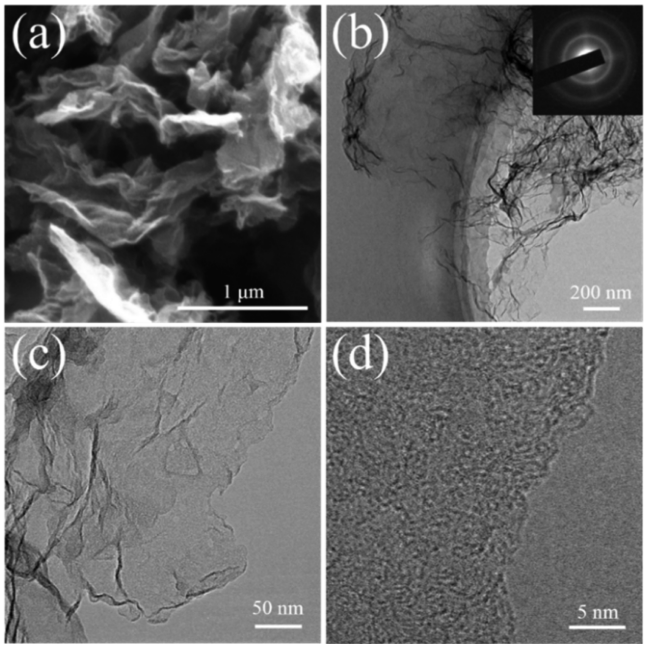

Figure 1. (a) SEM image of NG-C; (b) low-magnification TEM image and selected area electron diffraction (SAED) pattern (inset) of NG-C; (c) high-magnification TEM image of NG-C; (d) HRTEM image of NG-C.

diffraction (SAED) of the NG-C (inset of Figure 1b) shows a ring-like diffraction pattern of the typical hexagonal lattice of carbon, indicating the crystalline nature of N-doped graphene.[15] A HRTEM image shown in Figure 1d reveals the presence of disorder of the graphene domains with a size of a few nanometers. The morphologies of the NG-M and NG-T obtained from malic acid and tartaric acid, respectively, are similar to that of NG-C (SI Figures S3 and S4). An AFM image of the NG-C in Figure 2 reveals that the average thicknesses of the nanosheets are around 4 nm. The N-doped graphene has an average of about 12 atomic layers. Clearly the two-step

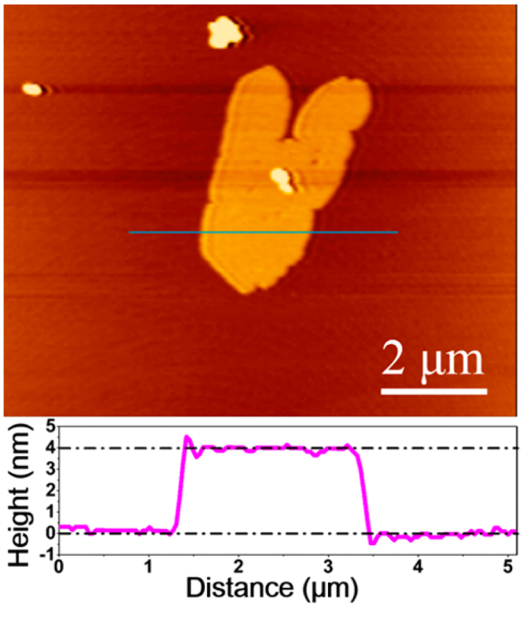

Figure 2. AFM image of NG-C.

calcination method by using AHAs as the carbon precursors and melamine as nitrogen source is effective for the fabrication of N-doped graphene with nanosheet structures.

The phases of the prepared samples were characterized using XRD. All three samples show a typical broad diffraction peak at 26° in their XRD patterns and which is indexed as (002) of the graphitic carbon, indicating an interlayer space of ~0.34 nm (Figure 3a). The structure and defect of the carbon materials are analyzed by Raman spectroscopy directly (Figure 3b). The two peaks at 1552 and 1586 cm^{-1} for the samples NG-M, NG-T, and NG-C correspond to the well-defined D band and G band, respectively. It is known that D band is caused by structural defects and partially disordered structures of graphene, while G band is related to the E_{2g} vibration mode of sp^2 carbon domains and can be used to estimate the degree of graphitization.[27] The intensity ratios of D band to G band (I_D/I_G) for NG-M, NG-T, and NG-C are all about 1.01, indicating the same structural defects, mainly caused by the N doping in the graphene frameworks.[19] The pore size and surface area are measured using nitrogen adsorption−desorption isotherms, and the results are shown in SI Figure S5. The textual parameters of the three N-doped graphene samples are summarized in Table 1. It is clear that the specific surface areas of NG-M, NG-T, and NG-C are 447, 1403, and 1167 $m^2\ g^{-1}$, respectively. The average pore sizes of NG-M, NG-T, and NG-C are calculated to be 9.92, 11.20, and 10.49 nm by using the Barrett−Joyner−Halenda (BJH) method, with the pore volumes of 1.11, 3.93, and 3.14 $cm^3\ g^{-1}$, respectively. These results confirm that the N-doped graphenes have high specific surface area (especially for NG-T and NG-C) and mesoporous structures.

XPS is performed to characterize the elemental composition and bonding configuration in the samples. The survey spectra shown in Figure 4a shows the presence of carbon (C 1s, 284.7 eV), nitrogen (N 1s, 400.8 eV), and oxygen (O 1s, 532.8 eV) in NG-M, NG-T, and NG-C. Generally, the C 1s peak of pristine graphene is at 284.5 eV, and the upshift of binding energy is evidence for the existence of N-doped carbon materials.[28] The high-resolution C 1s peaks of the three N-doped graphene samples (SI Figure S6) reveal a 0.2 eV upshift to 284.7 eV, indicating the formation of C−N bonds in the annealing process. N contents in the samples are calculated to be 4.12, 5.97, and 8.11 at. % for NG-M, NG-T, and NG-C, respectively (Table 1). Clearly, N-doped graphenes with different N contents can be obtained by using different AHAs. The XPS spectra of N 1s could be deconvoluted with three peaks at 398.2, 399.7, and 401.0 eV (Figure 4b) for pyridinic N, pyrrolic N, and quaternary N, respectively.[29] The amounts of the three N species in the samples are summarized and compared in Table 1. The contents of pyridinic N in NG-M, NG-T, and NG-C are 0.77, 1.55, and 3.02 at. %, respectively, and they follow the tendency of the total N content in the three samples. NG-C has the highest content of quaternary N at 4.35 at. %, while the content of quaternary N in NG-M (2.78 at. %) is slightly higher than that in NG-T (2.35 at. %). It has been reported that pyridinic N in a six-member ring donates one p-electron to the aromatic system. The pyrrolic N in the graphene layers forms five-member rings where it donates two p-electrons to the π-conjugated system. The quaternary nitrogens are the N atoms replacing the C atoms in the graphene hexagonal rings, and each of them connects with three carbon atoms in the graphene basal plane.[30] It has been shown that all of the N species play a remarkable effect on ORR activity of N-

DOI: 10.1021/acsami.5b05649
ACS Appl. Mater. Interfaces 2015, 7, 19619−19625

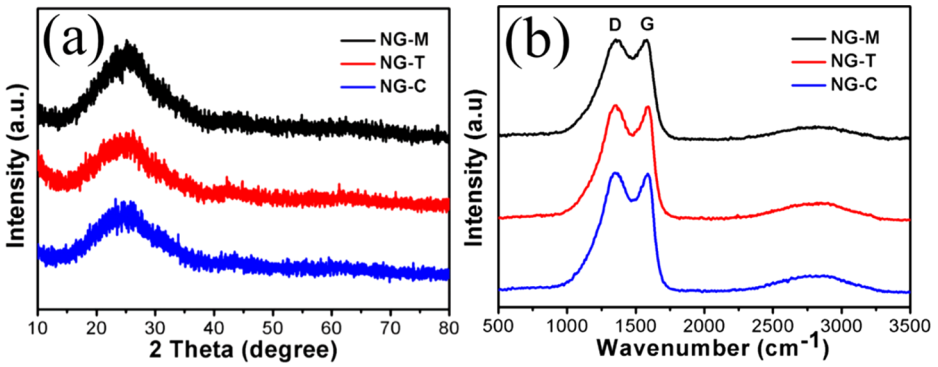

Figure 3. (a) XRD patterns and (b) Raman spectra of NG-M, NG-T, and NG-C.

Table 1. Textural Parameters of Nitrogen Sorption Analysis and XPS Analysis for Different N-Doped Graphenes

	nitrogen sorption analysis			XPS analysis			
sample	S_{BET} (m^2g^{-1})	pore vol. (cm^3 g^{-1})	pore size (nm)	total N content (at. %)	pyridinic N (at. %)	pyrrolic N (at. %)	quaternary N (at. %)
NG-M	447	1.11	9.92	4.17	0.77	0.62	2.78
NG-T	1403	3.93	11.20	5.97	1.55	2.07	2.35
NG-C	1167	3.14	10.49	8.11	3.02	0.74	4.35

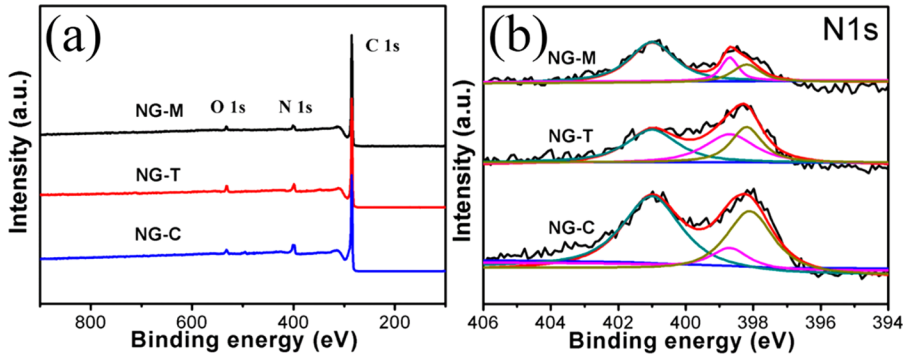

Figure 4. (a) XPS survey spectra of NG-M, NG-T, and NG-C; (b) XPS spectra of N 1s of NG-M, NG-T, and NG-C. The dark yellow, magenta, and green lines correspond to pyridinic N (398.2 eV), pyrrolic N (399.7 eV), and quaternary N (401.0 eV), respectively.

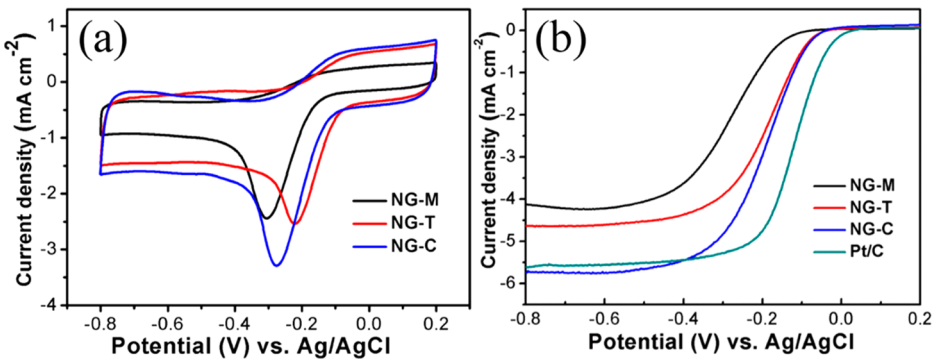

Figure 5. (a) CV plots of NG-M, NG-T, and NG-C in O_2-saturated 0.1 M KOH solution; (b) LSV curves of ORR on NG-M, NG-T, NG-C, and commercial Pt/C in O_2-saturated 0.1 M KOH solution at a scan rate of 5 mV/s at 1600 rpm.

doped graphene.[31] The XPS analysis results together with the XRD patterns and the Raman spectra have shown that N-doped graphenes were successfully synthesized.

Electrocatalytic Performances of N-Doped Graphenes for Oxygen Reduction Reaction. The catalytic activities of the N-doped graphenes for ORR are first evaluated by using cyclic voltammetry (CV) in an N_2-saturated or O_2-saturated 0.1 M KOH solution at a scan rate of 100 mV/s. SI Figure S7 shows that no obvious redox peaks can be observed when the electrolytes are saturated with N_2 for all of the samples. However, distinct reduction peaks appear when the solutions are saturated with O_2, indicating pronounced catalytic activity toward ORR. As shown in Figure 5a, the reduction peaks for NG-M, NG-T, and NG-C are located at −0.31, −0.22, and −0.28 V, respectively. The peak current density of NG-C (−3.3 mA cm^{-2}) is much higher than that of NG-M (−2.4 mA cm^{-2})

DOI: 10.1021/acsami.5b05649
ACS Appl. Mater. Interfaces 2015, 7, 19619−19625

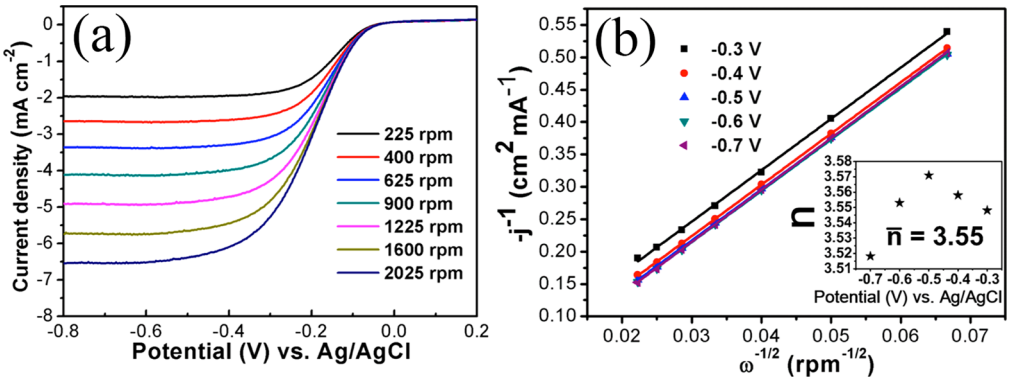

Figure 6. (a) LSV curves of ORR of NG-C obtained at different rotating rates; (b) K–L plots of current density reciprocal ($-j^{-1}$) versus $\omega^{-1/2}$ at different potentials on NG-C electrode. The insert is the transferred electron number (n) per oxygen molecule at different potentials. Note: the plots of −0.5, −0.6, and −0.7 V are overlapped.

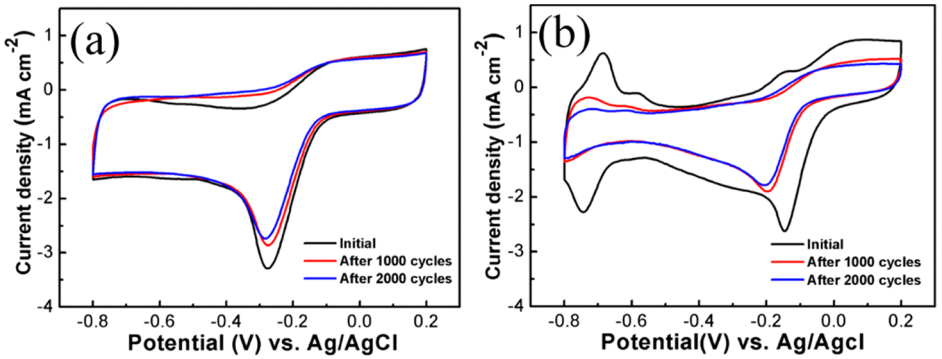

Figure 7. CV curve changes of (a) NG-C and (b) Pt/C in O_2-saturated 0.1 M KOH solution at a scan rate of 100 mV/s with 2000 cycles.

and NG-T (−2.6 mA cm^{-2}), indicating that the NG-C electrode can absorb and reduce more oxygen molecules on the surface. To further investigate the ORR activity, linear sweep voltammetry (LSV) curves were obtained from the rotating disk electrodes (RDE) of NG-M, NG-T, NG-C, and commercial 20 wt % Pt/C (Johnson Matthey, HiSPEC 3000) at a rotation rate of 1600 rpm, and the results are presented in Figure 5b. All of the samples show a typical one-stage process. The ORR onset potentials of both NG-T and NG-C were at about 0 V, which is more positive than that of NG-M (−0.07 V) and close to that of the Pt/C (0.04 V). The steady-state catalytic current density at the NG-C electrode is much higher than those of NG-M and NG-T, even a little higher than Pt/C over a large potential range, which makes it a potential candidate for the substitution of the commercial Pt/C. It is believed that the ORR activity of N-doped graphene mainly depends on the nitrogen content and N species in the carbon frameworks.[23] However, it is still not clear which type of nitrogen plays the most important role in the ORR activity. Some researchers claimed that quaternary N is responsible for the high ORR activity;[32,33] others stated that pyridinic N attributes most to the improved ORR activity.[34,35] In this work, we found that the ORR activities of NG-M, NG-T, and NG-C increase with the total N and pyridinic N contents in the three samples, even though the sample NG-C with the highest performance also has the highest quaternary N content (4.35 at. %). The ORR activity of NG-T containing 2.35 at. % quaternary N is better than that of NG-M which contains slightly higher quaternary N than that of NG-T at 2.78 at. % (see in Table 1 and Figure 5). On the basis of these results, it is reasonable to conclude that both the quaternary N and pyridinic N have positive effects on the ORR activity, but the pyridinic N seemed to play a key role.

The kinetics of the ORR activity of the best performance NG-C was further investigated at different rotating rates (from 225 to 2025 rpm). As shown in Figure 6a, the current density increases with the increase of the rotation rate. The corresponding Koutecky–Levich plots ($-J^{-1}$ vs $\omega^{-1/2}$) at various electrode potentials are presented in Figure 6b. It is clear that the K–L plots present good linearity. The slopes remain approximately constant over the potential range from −0.3 to −0.7 V, which suggests that the electron transfer numbers for oxygen reduction at different electrode potentials are similar. Linearity and parallelism of the K–L plots are usually regarded as an indication of first-order reaction kinetics with respect to the concentration of dissolved O_2.[36] The kinetic parameters are analyzed on the basis of the Koutecky–Levich equations:[37]

$$1/j = 1/j_k + 1/B\omega^{-1/2} \quad (1)$$

$$B = 0.2nF\upsilon^{-1/6}D_0^{2/3}C_0 \quad (2)$$

where j is the measured current density, j_k is the kinetic current density, B is the reciprocal of the slope, ω is the electrode rotating speed in rpm, n is the overall number of electrons transferred in oxygen reduction, F is the Faraday constant (F = 96485 C mol^{-1}), υ is the kinematic viscosity of the electrolyte (0.01 cm^2 s^{-1}), D_0 is the diffusion coefficient of O_2 in 0.1 M KOH (1.9×10^{-5} cm s^{-1}), and C_0 is the concentration of O_2 (1.2×10^{-3} mol L^{-1}). The constant 0.2 is adopted when the rotating speed is in rpm. Based on eqs 1 and 2, the average n

DOI: 10.1021/acsami.5b05649
ACS Appl. Mater. Interfaces 2015, 7, 19619–19625

was calculated to be 3.55 as shown in the inset of Figure 6b, closing to 4. This result reveals that the ORR activity of the NG-C catalyst follows the four electrons transfer pathway. We also performed continuous potential cycling to estimate the durability of the NG-C electrocatalyst toward ORR. As can be seen in Figure 7a, no significant decrease in current density is observed after 2000 cycles of NG-C in O_2-saturated 0.1 M KOH solution. On other hand, the current density decreases signficantly for the Pt/C electrode after 1000 cycles as shown in Figure 7b. The ORR performance after 2000 cycles for NG-C and commercial Pt/C were also obtained, corresponding to the results of CV curves (SI Figure S8). These results indicate NG-C has much better stability for ORR than the commercial Pt/C. All of these results demonstrate that the obtained NG-C is an ideal substitution for Pt/C.

CONCLUSION

In summary, a facile approach was developed for the fabrication of N-doped graphene via a two-step calcination strategy, by using AHAs as carbon sources and melamine as nitrogen source. By using different AHAs, N-doped graphenes with thin layered structure were successfully synthesized. The N contents in the resultant N-doped graphenes varied from 4.12 to 8.11 at. %. All of the resultant three N-doped graphenes (NG-M, NG-T, and NG-C) displayed high ORR activities. The better performance of NG-C than the commercial Pt/C is attributed to its high pyridinic N content. Further, NG-C also demonstrated good durability which makes it an ideal substitution of Pt/C.

ASSOCIATED CONTENT

Supporting Information

This material is available free of charge via the Internet at http://pubs.acs.org/. The Supporting Information is available free of charge on the ACS Publications website at DOI: 10.1021/acsami.5b05649.

Molecular formulas of malic acid, tartaric acid, and citric acid, XRD pattern and SEM image of g-C3N4, SEM and TEM images of NG-M and NG-T, BET characterization and XPS C 1s spectra of NG-M, NG-T, and NG-C, CV plots of NG-M, NG-T, and NG-C in N_2-saturated or O_2-saturated 0.1 M KOH solution, and ORR forward peak maximum currents for NG-C and Pt/C (PDF)

AUTHOR INFORMATION

Corresponding Author

*E-mail: smzhu@sjtu.edu.cn.

Author Contributions

⊥Y.L. and Y.G. contributed equally to this work.

Notes

The authors declare no competing financial interest.

ACKNOWLEDGMENTS

We gratefully acknowledge financial support for this research from the National Science Foundation of China (Grant Nos. 51072117 and 51171110), the National Basic Research Program of China (973 Program, Grant 2012CB619600), and the Shanghai Science and Technology Committee (Grants 10JC1407600 and 13JC1403300). We also thank SJTU Instrument Analysis Center for the measurements.

REFERENCES

(1) Xu, X.; Yuan, T.; Zhou, Y.; Li, Y.; Lu, J.; Tian, X.; Wang, D.; Wang, J. Facile Synthesis of Boron and Nitrogen-Doped Graphene as Efficient Electrocatalyst for the Oxygen Reduction Reaction in Alkaline Media. *Int. J. Hydrogen Energy* **2014**, *39*, 16043−16052.

(2) Qu, L.; Liu, Y.; Baek, J.-B.; Dai, L. Nitrogen-Doped Graphene as Efficient Metal-Free Electrocatalyst for Oxygen Reduction in Fuel Cells. *ACS Nano* **2010**, *4*, 1321−1326.

(3) Paulus, U.; Wokaun, A.; Scherer, G.; Schmidt, T.; Stamenkovic, V.; Radmilovic, V.; Markovic, N.; Ross, P. Oxygen Reduction on Carbon-Supported Pt-Ni and Pt-Co Alloy Catalysts. *J. Phys. Chem. B* **2002**, *106*, 4181−4191.

(4) Alegre, C.; Gálvez, M.; Moliner, R.; Baglio, V.; Aricò, A.; Lázaro, M. Towards an Optimal Synthesis Route for the Preparation of Highly Mesoporous Carbon Xerogel-Supported Pt Catalysts for the Oxygen Reduction Reaction. *Appl. Catal., B* **2014**, *147*, 947−957.

(5) Fang, B.; Chaudhari, N. K.; Kim, M.-S.; Kim, J. H.; Yu, J.-S. Homogeneous Deposition of Platinum Nanoparticles on Carbon Black for Proton Exchange Membrane Fuel Cell. *J. Am. Chem. Soc.* **2009**, *131*, 15330−15338.

(6) Kim, J. H.; Fang, B.; Song, M. Y.; Yu, J.-S. Topological Transformation of Thioether-Bridged Organosilicas into Nanostructured Functional Materials. *Chem. Mater.* **2012**, *24*, 2256−2264.

(7) Wang, Y.-J.; Zhao, N.; Fang, B.; Li, H.; Bi, X. T.; Wang, H. Carbon-Supported Pt-Based Alloy Electrocatalysts for the Oxygen Reduction Reaction in Polymer Electrolyte Membrane Fuel Cells: Particle Size, Shape, and Composition Manipulation and Their Impact to Activity. *Chem. Rev.* **2015**, *115*, 3433−3467.

(8) Debe, M. K. Electrocatalyst Approaches and Challenges for Automotive Fuel Cells. *Nature* **2012**, *486*, 43−51.

(9) Fei, H.; Ye, R.; Ye, G.; Gong, Y.; Peng, Z.; Fan, X.; Samuel, E. L.; Ajayan, P. M.; Tour, J. M. Boron-and Nitrogen-Doped Graphene Quantum Dots/Graphene Hybrid Nanoplatelets as Efficient Electrocatalysts for Oxygen Reduction. *ACS Nano* **2014**, *8*, 10837−10843.

(10) Westervelt, R. Graphene Nanoelectronics. *Science* **2008**, *320*, 324−325.

(11) Pumera, M. Graphene-Based Nanomaterials for Energy Storage. *Energy Environ. Sci.* **2011**, *4*, 668−674.

(12) Wang, D.; Min, Y.; Yu, Y.; Peng, B. A General Approach for Fabrication of Nitrogen-Doped Graphene Sheets and Its Application in Supercapacitors. *J. Colloid Interface Sci.* **2014**, *417*, 270−277.

(13) Le, L. T.; Ervin, M. H.; Qiu, H.; Fuchs, B. E.; Lee, W. Y. Graphene Supercapacitor Electrodes Fabricated by Inkjet Printing and Thermal Reduction of Graphene Oxide. *Electrochem. Commun.* **2011**, *13*, 355−358.

(14) Lu, C. H.; Yang, H. H.; Zhu, C. L.; Chen, X.; Chen, G. N. A Graphene Platform for Sensing Biomolecules. *Angew. Chem.* **2009**, *121*, 4879−4881.

(15) Sheng, Z.-H.; Shao, L.; Chen, J.-J.; Bao, W.-J.; Wang, F.-B.; Xia, X.-H. Catalyst-Free Synthesis of Nitrogen-Doped Graphene via Thermal Annealing Graphite Oxide with Melamine and Its Excellent Electrocatalysis. *ACS Nano* **2011**, *5*, 4350−4358.

(16) Chen, P.; Wang, L. K.; Wang, G.; Gao, M. R.; Ge, J.; Yuan, W. J.; Shen, Y.; Xie, A.; Yu, S. H. Nitrogen-Doped Nanoporous Carbon Nanosheets Derived from Plant Biomass: An Efficient Catalyst for Oxygen Reduction Reaction. *Energy Environ. Sci.* **2014**, *7*, 4095−4103.

(17) Chen, P.; Xiao, T. Y.; Qian, Y. H.; Li, S. S.; Yu, S. H. A Nitrogen-Doped Graphene/Carbon Nanotube Nanocomposite with Synergistically Enhanced Electrochemical Activity. *Adv. Mater.* **2013**, *25*, 3192−3196.

(18) Yuan, W.; Li, J.; Wang, L.; Chen, P.; Xie, A.; Shen, Y. Nanocomposite of N-Doped TiO_2 Nanorods and Graphene as An Effective Electrocatalyst for Oxygen Reduction Reaction. *ACS Appl. Mater. Interfaces* **2014**, *6*, 21978−21985.

(19) Cong, H.-P.; Wang, P.; Gong, M.; Yu, S.-H. Facile Synthesis of Mesoporous Nitrogen-Doped Graphene: An Efficient Methanol-Tolerant Cathodic Catalyst for Oxygen Reduction Reaction. *Nano Energy* **2014**, *3*, 55−63.

DOI: 10.1021/acsami.5b05649
ACS Appl. Mater. Interfaces 2015, 7, 19619−19625

(20) Luo, Z.; Lim, S.; Tian, Z.; Shang, J.; Lai, L.; MacDonald, B.; Fu, C.; Shen, Z.; Yu, T.; Lin, J. Pyridinic N doped Graphene: Synthesis, Electronic Structure, and Electrocatalytic Property. *J. Mater. Chem.* **2011**, *21*, 8038−8044.
(21) Wei, D.; Liu, Y.; Wang, Y.; Zhang, H.; Huang, L.; Yu, G. Synthesis of N-Doped Graphene by Chemical Vapor Deposition and Its Electrical Properties. *Nano Lett.* **2009**, *9*, 1752−1758.
(22) Liang, J.; Jiao, Y.; Jaroniec, M.; Qiao, S. Z. Sulfur and Nitrogen Dual-Doped Mesoporous Graphene Electrocatalyst for Oxygen Reduction with Synergistically Enhanced Performance. *Angew. Chem., Int. Ed.* **2012**, *51*, 11496−11500.
(23) Geng, D.; Chen, Y.; Chen, Y.; Li, Y.; Li, R.; Sun, X.; Ye, S.; Knights, S. High Oxygen-Reduction Activity and Durability of Nitrogen-Doped Graphene. *Energy Environ. Sci.* **2011**, *4*, 760−764.
(24) Li, X. H.; Kurasch, S.; Kaiser, U.; Antonietti, M. Synthesis of Monolayer-Patched Graphene from Glucose. *Angew. Chem., Int. Ed.* **2012**, *51*, 9689−9692.
(25) Li, X. H.; Antonietti, M. Polycondensation of Boron-and Nitrogen-Codoped Holey Graphene Monoliths from Molecules: Carbocatalysts for Selective Oxidation. *Angew. Chem., Int. Ed.* **2013**, *52*, 4572−4576.
(26) Tian, J.; Liu, Q.; Asiri, A. M.; Al-Youbi, A. O.; Sun, X. Ultrathin Graphitic Carbon Nitride Nanosheet: A Highly Efficient Fluorosensor for Rapid, Ultrasensitive Detection of Cu2+. *Anal. Chem.* **2013**, *85*, 5595−5599.
(27) Allen, M. J.; Tung, V. C.; Kaner, R. B. Honeycomb Carbon: A Review of Graphene. *Chem. Rev.* **2010**, *110*, 132−145.
(28) Choi, C. H.; Chung, M. W.; Kwon, H. C.; Chung, J. H.; Woo, S. I. Nitrogen-Doped Graphene/Carbon Nanotube Self-Assembly for Efficient Oxygen Reduction Reaction in Acid Media. *Appl. Catal., B* **2014**, *144*, 760−766.
(29) Maldonado, S.; Morin, S.; Stevenson, K. J. Structure, Composition, and Chemical Reactivity of Carbon Nanotubes by Selective Nitrogen Doping. *Carbon* **2006**, *44*, 1429−1437.
(30) Vikkisk, M.; Kruusenberg, I.; Joost, U.; Shulga, E.; Kink, I.; Tammeveski, K. Electrocatalytic Oxygen Reduction on Nitrogen-Doped Graphene in Alkaline Media. *Appl. Catal., B* **2014**, *147*, 369−376.
(31) Wang, H.; Maiyalagan, T.; Wang, X. Review on Recent Progress in Nitrogen-Doped Graphene: Synthesis, Characterization, and Its Potential Applications. *ACS Catal.* **2012**, *2*, 781−794.
(32) Nagaiah, T. C.; Kundu, S.; Bron, M.; Muhler, M.; Schuhmann, W. Nitrogen-Doped Carbon Nanotubes as a Cathode Catalyst for the Oxygen Reduction Reaction in Alkaline Medium. *Electrochem. Commun.* **2010**, *12*, 338−341.
(33) Niwa, H.; Horiba, K.; Harada, Y.; Oshima, M.; Ikeda, T.; Terakura, K.; Ozaki, J.-i.; Miyata, S. X-Ray Absorption Analysis of Nitrogen Contribution to Oxygen Reduction Reaction in Carbon Alloy Cathode Catalysts for Polymer Electrolyte Fuel Cells. *J. Power Sources* **2009**, *187*, 93−97.
(34) Kundu, S.; Nagaiah, T. C.; Xia, W.; Wang, Y.; Dommele, S. V.; Bitter, J. H.; Santa, M.; Grundmeier, G.; Bron, M.; Schuhmann, W.; Muhler, M. Electrocatalytic Activity and Stability of Nitrogen-Containing Carbon Nanotubes in the Oxygen Reduction Reaction. *J. Phys. Chem. C* **2009**, *113*, 14302−14310.
(35) Sun, Y.; Li, C.; Shi, G. Nanoporous Nitrogen Doped Carbon Modified Graphene as Electrocatalyst for Oxygen Reduction Reaction. *J. Mater. Chem.* **2012**, *22*, 12810−12816.
(36) Liu, R.; Wu, D.; Feng, X.; Müllen, K. Nitrogen-Doped Ordered Mesoporous Graphitic Arrays with High Electrocatalytic Activity for Oxygen Reduction. *Angew. Chem.* **2010**, *122*, 2619−2623.
(37) Lin, Z.; Waller, G. H.; Liu, Y.; Liu, M.; Wong, C.-P. 3D Nitrogen-Doped Graphene Prepared by Pyrolysis of Graphene Oxide with Polypyrrole for Electrocatalysis of Oxygen Reduction Reaction. *Nano Energy* **2013**, *2*, 241−248.

DOI: 10.1021/acsami.5b05649
ACS Appl. Mater. Interfaces 2015, 7, 19619−19625